E-ISSN: 2707-8299
P-ISSN: 2707-8280
Journal's Website
IJSDE 2024; 5(2): 34-42
Received: 20-06-2024
Accepted: 26-07-2024

Vincenzo De Luca
Department D.I.S., University of Basilicata, Viale dell'Ateneo Lucano 10, Potenza 85100, Italy

Cosimo Marano
S.A.F.E., University of Basilicata, Viale dell'Ateneo Lucano 10, Potenza 85100, Italy

Corresponding Author:
Vincenzo De Luca
Department D.I.S., University of Basilicata, Viale dell'Ateneo Lucano 10, Potenza 85100, Italy

A finite element method with inter-element interpolation points for thin plate. Part II: Mixed formulation

Vincenzo De Luca and Cosimo Marano

DOI: https://doi.org/10.22271/27078280.2024.v5.i2a.34

Abstract
This study introduces a new mixed finite element formulation for the analysis of elastic thin plates, incorporating inter-element interpolation points for enhanced performance and implementation simplicity. The method utilizes a regular rectangular mesh, where the displacement field is interpolated using bi-quadratic functions, and the stress field is approximated through bi-linear interpolation. The quadratic interpolation for displacements is flexibly defined by adjusting the positions of control points, which can be located within, on the boundaries, or outside, of the mesh elements. This approach ensures continuity across mesh elements while reducing the degrees of freedom in the discretized system of equations.
The governing equations are derived by enforcing the stationary of the mixed Hellinger–Reissner functional. Numerical applications are conducted for isotropic, linearly elastic thin plates subjected to different loading conditions and boundary conditions. The numerical results demonstrate the high accuracy of the proposed method in reproducing displacement and stress fields, showing excellent agreement with analytical solutions and validating its effectiveness.

Keywords: Finite element method, mixed finite element method, elastic analysis of thin plate, element interpolation points, bending thin plate

Introduction
The most widely used finite element methods (FEM) are compatible-type models, which assume kinematic variables as the primary unknowns. These models deliver accurate approximations for kinematic quantities but often fail to achieve a balanced accuracy between displacement and stress fields (Bathe, 1996) [1].
To address these limitations, several alternative formulations have been developed and proposed in the literature. Among these are assumed-stress formulations (Pian, 1964; Pian and Sumihara, 1984) [2, 3] and as well as strain-based formulations (Simo and Rifai, 1990; Bergan and Felippa, 1991) [4, 5], which have been applied to thin and thick plates (Boussem *et al*., 2020) [6] and shells (Rebiai *et al*., 2014) [7]. Smoothing techniques, which approximate average strain (Liu *et al*., 2009a, 2009b) [8, 9], and elements employing high-degree interpolations (Zienkiewicz and Taylor, 2000a, 2000b) [10, 11] have also been utilized. However, many of these methods suffer from issues such as shear locking or spurious zero-energy modes in thin structures. To mitigate these issues, reduced integration techniques for shear terms and specialized plate elements have been introduced. Despite their benefits, these methods are often complex and computationally intensive, limiting their adoption in standard FEM codes. Mixed and hybrid element formulations have also been explored (Pian and Tong, 1969; Lee and Pian, 1978; Lee and Wong, 1982; Leonetti and Aristodemo, 2015; Bilotta and Casciaro, 2007) [12-16] to address the limitations of compatible models.
This paper introduces a mixed FEM formulation for thin plates. The proposed method adopts separate interpolation strategies for displacements and moments, to achieve a balanced representation of kinematic and static variables. A novel inter-element continuity technique is employed for displacement interpolation, using bi-quadratic functions to ensure continuity of both the function and its derivatives. For moment interpolation, a bi-linear form is utilized.
The mixed model is developed by applying the minimum principle of the Hellinger–Reissner functional, resulting in a straightforward formulation for discrete elements.

Numerical tests on static elastic linear of thin plates are conducted to validate the model's accuracy and robustness.

Materials and Methods

Theory

The numerical analysis presented in this study pertains to the bending of thin plates based on Kirchhoff's theory. The plate is modeled as a two-dimensional, plane domain with elastic, linear, homogeneous, and isotropic material properties. The analysis considers a thin plate of thickness h, with a volume domain V and boundary surface S, subjected to a transverse load $p(x,y)$. A Cartesian coordinate system (O,x,y,z) is employed, with the x and y axes lying on the mid-plane of the plate, and the z axis orthogonal to this plane (Figure 1).

The bending behavior is described only in terms of the transverse displacement $u_z(x,y)$, while shear deformations are assumed negligible (Szilard, 1974; Timoshenko and Woinowsky-Krieger, 1984) [17, 18]. The theoretical framework is governed by Kirchhoff's hypotheses, defining the kinematic deformation model:

- Rectilinear normals to the mid-plane remain conserved, with zero shear strains γ_{zx} and γ_{zy};
- linear extensional strains ε_x and ε_y vary linearly across the thickness, with a neutral axis at the mid-plane;
- transverse displacement $u_z(x,y)$ is infinitesimally small along z axes;
- the normal stress component σ_{zz} is considered negligible in comparison to the components σ_{xx} and σ_{yy}.

The compatibility equations corresponding to the kinematic hypotheses are found as follows.

The rotations φ_x and φ_y about the $x-axes$ and $y-axes$, respectively, are expressed as partial derivates of the transverse displacement:

$$\varphi_x = -\frac{\partial u_z}{\partial x} \quad (1)$$

$$\varphi_y = -\frac{\partial u_z}{\partial y}. \quad (2)$$

From these, the displacement components u_x and u_y are derived:

$$u_x = z \cdot \varphi_x = -z \cdot \frac{\partial u_z}{\partial x}, \quad (3)$$

$$u_y = z \cdot \varphi_y = -z \cdot \frac{\partial u_z}{\partial y}, \quad (4)$$

where

u_z is the vertical deflection, the variables φ_x and φ_y represent the rotations about the y and x axes, respectively.

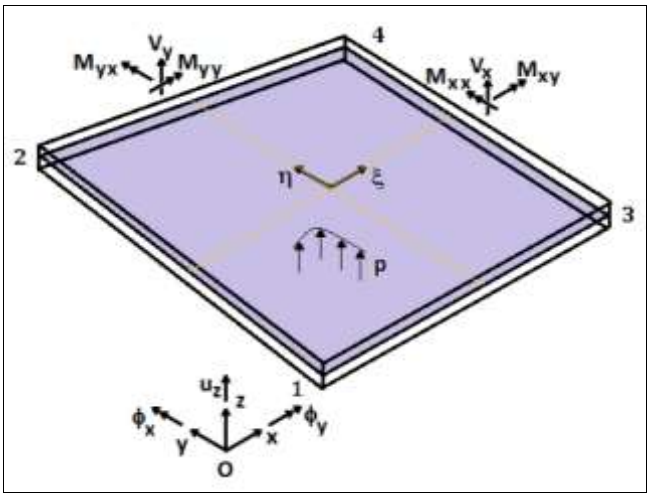

Fig 1: The variables associated with the Kirchhoff plate are defined within the reference coordinate system.

The strain components are given by:

$$\varepsilon_{xx} = \frac{\partial u}{\partial x} = -z \cdot \frac{\partial^2 u_z}{\partial x^2}, \quad (5)$$

$$\varepsilon_{yy} = \frac{\partial u}{\partial y} = -z \cdot \frac{\partial^2 u_z}{\partial y^2}, \quad (6)$$

$$\gamma_{xy} = \frac{\partial u}{\partial y} + \frac{\partial u}{\partial x} = -2 \cdot z \cdot \frac{\partial^2 u_z}{\partial x \partial y} \quad (7)$$

The stress components for a linear, isotropic elastic material are:

$$\sigma_{xx} = \frac{E}{1-\upsilon^2} \cdot (\varepsilon_x + \upsilon \cdot \varepsilon_y) = -\frac{E}{1-\upsilon^2} \cdot z \cdot \left(\frac{\partial^2 u_z}{\partial x^2} + \upsilon \cdot \frac{\partial^2 u_z}{\partial y^2}\right) \quad (8)$$

$$\sigma_{yy} = \frac{E}{1-\upsilon^2} \cdot (\upsilon \cdot \varepsilon_x + \varepsilon_y) = -\frac{E}{1-\upsilon^2} \cdot z \cdot \left(\upsilon \cdot \frac{\partial^2 u_z}{\partial x^2} + \frac{\partial^2 u_z}{\partial y^2}\right) \quad (9)$$

$$\tau_{xy} = \frac{E}{2 \cdot (1+\upsilon)} \cdot \gamma_{xy} = -\frac{E}{1-\upsilon^2} \cdot z \cdot \frac{\partial^2 u_z}{\partial x \partial y}. \quad (10)$$

By performing an integration of the stress components across the thickness of the plate, the resulting bending moments are obtained as follows:

$$M_{xx} = \int_{-\frac{h}{2}}^{\frac{h}{2}} \sigma_x \cdot z \cdot dz = -\frac{E \cdot h}{12 \cdot (1-\upsilon^2)} \cdot \left(\frac{\partial^2 u_z}{\partial x^2} + \upsilon \cdot \frac{\partial^2 u_z}{\partial y^2}\right), \quad (11)$$

$$M_{yy} = \int_{-\frac{h}{2}}^{\frac{h}{2}} \sigma_y \cdot z \cdot dz = -\frac{E \cdot h}{12 \cdot (1-\upsilon^2)} \cdot \left(\upsilon \cdot \frac{\partial^2 u_z}{\partial x^2} + \frac{\partial^2 u_z}{\partial y^2}\right), \quad (12)$$

$$M_{xy} = \int_{-\frac{h}{2}}^{\frac{h}{2}} \sigma_x \cdot z \cdot dz = -\frac{E \cdot h}{12 \cdot (1-\upsilon^2)} \cdot (1-\upsilon) \cdot \frac{\partial^2 u_z}{\partial x \partial y} \quad (13)$$

The transverse shear forces are obtained from the rotational equilibrium equations:

$$V_x = -\frac{E \cdot h}{12 \cdot (1-\upsilon^2)} \cdot \left(\frac{\partial^3 u_z}{\partial x^3} + \frac{\partial^3 u_z}{\partial x \partial y^2}\right), \quad (14)$$

$$V_y = -\frac{E \cdot h}{12 \cdot (1-\upsilon^2)} \cdot \left(\frac{\partial^3 u_z}{\partial x^2 \partial y} + \frac{\partial^3 u_z}{\partial y^2 \partial x}\right). \quad (15)$$

The equilibrium equation for the plate is:

$$\frac{\partial^4 u_z}{\partial x^4} + 2 \cdot \frac{\partial^4 u_z}{\partial x^2 \partial y^2} + \frac{\partial^4 u_z}{\partial y^4} = \frac{p}{D} \quad (16)$$

where

$$D = \frac{E \cdot h^3}{12 \cdot (1-\upsilon^2)} \text{ is the flexural rigidity;} \quad (17)$$

E is the elastic modulus;

υ is the Poisson's coefficient.

Mixed FEM model construction

The Hellinger–Reissner principle is employed, its mixed formulation incorporates the following quantities:

$\underline{m} = \begin{bmatrix} m_x \\ m_y \\ m_{xy} \end{bmatrix}$: array of moments;

$\underline{u} = [u_z]$: array of displacement;

$\underline{p} = [p]$: array of bulk loads;

$\underline{\bar{t}}^T = [\bar{t}]$: array of surface loads;

$\underline{\chi} = \begin{bmatrix} \chi_x \\ \chi_y \\ \chi_{xy} \end{bmatrix}$: array of curvature;

Assuming the plate is composed of a homogeneous material with a constant thickness, the averaged bending moment, integrated across the plate's thickness, is expressed by the following fundamental relationships:

$$\underline{m} = \mathbf{E} \cdot \underline{\chi}, \quad (18)$$

Where

$\mathbf{E} = \frac{E \cdot h^3}{12 \cdot (1-\upsilon^2)} \cdot \begin{bmatrix} 1 & \upsilon & 0 \\ \upsilon & 1 & 0 \\ 0 & 0 & \frac{1-\upsilon}{2} \end{bmatrix}$ is the bending stiffness matrix (19)

From the displacement vector, $\underline{u}$, the curvature vector, $\underline{\chi}$, of the thin plate can be easily computed by applying the differential operator, D.

$$\mathbf{D} = \left[\frac{\partial^2}{\partial x^2} \quad \frac{\partial^2}{\partial x^2} \quad 2 \cdot \frac{\partial^2}{\partial x \partial y}\right]^T \quad (20)$$

to the displacement vector, $\underline{u}$, as follows:

$$\underline{\chi} = \begin{bmatrix} \chi_{xx} \\ \chi_{xx} \\ \chi_{xy} \end{bmatrix} = -\begin{bmatrix} \frac{\partial^2 u_z}{\partial x^2} \\ \frac{\partial^2 u_z}{\partial x^2} \\ 2 \cdot \frac{\partial^2 u_z}{\partial x \partial y} \end{bmatrix} = -\mathbf{D} \cdot \underline{u} \quad (21)$$

The differential operator, $\mathbf{D}$, being a second-order partial differential operator, requires that the displacement function $\underline{u}$ must be at least twice differentiable.

The Hellinger–Reissner functional for thin plates is expressed as:

$$\Pi_R(\underline{u}, \underline{m}) = -\frac{1}{2}\int_V \underline{m}^T \cdot \mathbf{E}^{-1} \cdot \underline{m} \cdot dV + \int_V \underline{m}^T \cdot \mathbf{D} \cdot \underline{u} \cdot dV - \int_V \underline{p}^T \cdot \underline{u} \cdot dV - \int_{S_\sigma} \underline{\bar{t}}^T \cdot \delta \underline{u} \cdot dS - \int_{S_\sigma} \underline{\bar{t}}^T \cdot (\underline{u} - \underline{\bar{u}}) \cdot dS \quad (22)$$

It is assumed that boundary conditions are imposed on the displacements so that it results

$$\underline{u} = \underline{\bar{u}} \text{ on } S_\upsilon, \quad (23)$$

thus canceling the term on S_u in the functional and leaving the conditions on the tensions as natural.

The functional (22) is discretized using appropriate interpolations for displacement and moment fields. Displacement field, requiring continuity within and between the elements of the mesh, is interpolated using bi-quadratic functions, while moment fields, not constrained by continuity (Pian and Sumihara, 1984) [4], are interpolated using bi-linear functions.

Interpolation of the transverse displacement with quadratic elements

The physical domain is discretized into a rectangular grid (Figures 1 and 2) with mesh dimensions $a \times b$. Each element is represented by the geometry defined by its nodal coordinates $x_i, y_i, i = 1,2,3,4$. A local coordinate system, denoted by ξ and η, is introduced with its origin at the center of the element. In this system, the dimensionless coordinates are defined as follows:

$$\xi = \frac{x}{a}, \quad (24)$$

$$\eta = \frac{y}{b}. \quad (25)$$

The displacement field $\underline{u}(\xi, \eta)$ is interpolated using a quadratic formulation:

$$\underline{u}(\xi, \eta) = \mathbf{A}(\xi, \eta) \cdot \underline{U}, \quad (26)$$

where $\mathbf{A}$ is the shape function matrix linking the displacement at the current point within the element to the global vector of nodal parameters $\underline{U}$.

The matrix $\mathbf{A}$ for a generic element depends on the nine nodal parameters $U_{11}, U_{12}, \ldots U_{33}$ of the element and its adjacent elements, as:

$$\mathbf{A}(\xi,\eta)\cdot\underline{U} = u_z(\xi,\eta) = \sum_{i=1}^{3}\sum_{i=1}^{3}\phi_i(\xi)\cdot\phi_j(\eta)\cdot U_{ij}. \quad (27)$$

Here, $\phi_i(\xi)$ and $\phi_j(\eta)$ are one-dimensional shape functions corresponding to the dimensionless coordinates, describing the position of the nodal parameter concerning the center of the element. We consider ξ and η equal to $\frac{1}{2}$ and 0 at a boundary edges.

Bilinear interpolation of moments

To construct the mixed model, the stress characteristics, moments, are interpolated independently using a bilinear form. The basic interpolation assumed for the moments field $\underline{m}(\xi,\eta)$ is given in the following form:

$$\underline{m}(\xi,\eta) = \mathbf{B}(\xi,\eta)\cdot\underline{M}, \quad (28)$$

where $\mathbf{B}$ is the shape function matrix linking the moments $\underline{m}$ to the global vector $\underline{M}$ of nodal moment parameters.

For a bilinear form, the moments in a generic element follow the scheme in Figure 2, with nodal variables located at the vertices of the element. The vector of moment components is:

$$\underline{m} = \begin{bmatrix} m_{xx} \\ m_{yy} \\ m_{xy} \end{bmatrix} \quad (29)$$

whose components are interpolated as:

$$m_{xx}(\xi,\eta) = \sum_{j=1}^{2}\sum_{i=1}^{2}\Psi_j(\xi)\cdot\Psi(\eta)\cdot M_{xij}, \quad (30)$$

$$m_{yy}(\xi,\eta) = \sum_{j=1}^{2}\sum_{i=1}^{2}\Psi_j(\xi)\cdot\Psi(\eta)\cdot M_{yij}, \quad (31)$$

$$m_{xy}(\xi,\eta) = \sum_{j=1}^{2}\sum_{i=1}^{2}\Psi_j(\xi)\cdot\Psi(\eta)\cdot M_{xyij}. \quad (32)$$

The linear shape functions are:

$$\Psi_1(\xi) = \frac{1}{2} - \xi, \quad (33)$$

$$\Psi_2(\xi) = \frac{1}{2} + \xi, \quad (34)$$

$$\Psi_1(\eta) = \frac{1}{2} - \eta, \quad (35)$$

$$\Psi_2(\eta) = \frac{1}{2} - \eta. \quad (36)$$

Discretized equations

Substituting the interpolated shapes (26) and (28) into the functional in Equations (22)–(23) yields the discretized functional:

$$\Pi = -\frac{1}{2}\underline{M}^T\cdot\mathbf{F}\cdot\underline{M} + \underline{M}^T\cdot\mathbf{G}\cdot\underline{M} - \underline{U}^T\cdot\underline{P}, \quad (37)$$

where the following assembled arrays are defined:

$$\mathbf{F} = \int_V \mathbf{B}^T\cdot\mathbf{E}\cdot\mathbf{B}\cdot dV, \text{ the flexibility matrix,} \quad (38)$$

$$\mathbf{G} = \int_V \mathbf{B}^T\cdot\mathbf{D}\cdot\mathbf{A}\cdot dV, \text{ the compatibility matrix,} \quad (39)$$

$$\underline{P} = \int_V \mathbf{A}^T\cdot\underline{p}\cdot dS + \int_{S_\sigma}\mathbf{A}^T\cdot\bar{\underline{t}}\cdot dS, \text{ the equivalent load vector associated with the nodal displacement parameters.} \quad (40)$$

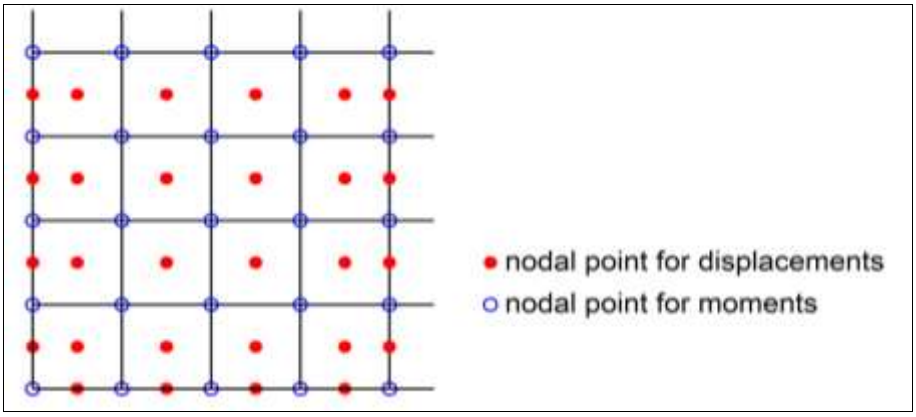

Fig 2: Scheme of the mesh with the nodal point for displacement and moments.

To find the stationary conditions for the functional, the minimum conditions are imposed concerning the nodal displacement vector and the nodal moment vector:

$$\frac{\partial \Pi_R}{\partial \underline{U}} = 0 \rightarrow \underline{M}^T \cdot \mathbf{G} - \underline{P} = \underline{0} \quad (41)$$

$$\frac{\partial \Pi_R}{\partial \underline{M}} = 0 \rightarrow -\mathbf{F} \cdot \underline{M} + \mathbf{G} \cdot \underline{U} = \underline{0} \quad (42)$$

This results in the linear system:

$$\begin{bmatrix} -\mathbf{F} & \mathbf{G} \\ \mathbf{G}^T & \mathbf{0} \end{bmatrix} \cdot \begin{bmatrix} \underline{M} \\ \underline{U} \end{bmatrix} = \begin{bmatrix} \underline{0} \\ \underline{P} \end{bmatrix} \quad (43)$$

The formulation can be reduced to a system of equations in terms of the kinematic unknowns only, by eliminating the static unknowns M:

$$\mathbf{K_m} = \mathbf{G}^T \cdot \mathbf{F}^{-1} \cdot \mathbf{G} \quad (44)$$

Imposing boundary conditions

The boundary conditions are imposed on both the displacement and rotation fields, ensuring the appropriate constraints are applied at the boundaries of the domain. The displacement boundary conditions are imposed directly on the nodal displacement vector $\underline{U}$. Rotational boundary restrictions are enforced on the nodal displacement as follows:

$$\varphi_x(\xi,\eta) = -\frac{\partial u_z}{\partial \xi} = -\sum_{j=1}^{3}\sum_{i=1}^{3} \frac{\partial \phi_i(\xi)}{\partial \xi} \cdot \phi_j(\eta) \cdot U_{ij} \quad (45)$$

$$\varphi_y(\xi,\eta) = -\frac{\partial u_z}{\partial \eta} = -\sum_{j=1}^{3}\sum_{i=1}^{3} \phi_i(\xi) \cdot \frac{\partial \phi_j(\xi)}{\partial \eta} \cdot U_{ij} \quad (46)$$

Numerical analysis

The computational procedure is applied to classic problems involving square plates with various boundary conditions, including simply supported and fully clamped edges.

Square Plate

The analyzed square plate has dimensions $a = 1000\ mm$ and $b = 1000\ mm$, thickness $h = 2\ mm$, and has mechanical characteristics elastic modulus $E = 2.1 \cdot 10^4\ daN/mm^2$ and Poisson's ratio $\upsilon = 0.3$. Numerical results are evaluated for different configurations and loading conditions.

Results and discussion

Tables 1 through 4 summarize the key outcomes of the numerical analysis, including the central displacement, the bending moment at the center, and the moment at the midpoint of the edge for a fully clamped plate. The performance of the proposed finite element formulation is evaluated by comparing the numerical results with analytical solutions derived from plate bending theory. For the simply supported plate, the analytical solution employs a double Fourier series truncated at the 11th term. For the other boundary condition, a single-term Fourier series is used.

The numerical results are presented according to different levels of mesh refinement, enabling a direct assessment of the method's convergence behavior. This comparison highlights the ability of the proposed method to approximate exact solutions as the mesh becomes finer.

Table 1 presents the results for a square plate simply supported under a uniform load. The dimensionless central deflection, central moment, and the moment at the middle edge (theoretically zero) are reported alongside their relative errors. Figures 3 and 4 illustrate the trends in relative errors for the central deflection and moment, comparing the compatible and mixed models. For a 26 x 26 mesh, relative errors reduce to approximately 0.01% for central deflection and 1.32% for the central moment. The results demonstrate that even with a minimal number of integration points, the proposed thin plate elements achieve high accuracy.

Table 1: Square plate supported on four edges, subjected to uniform load.

Mesh	d.o.f.	o	$\alpha/(\alpha-\alpha_a)$	ß	$\beta/(\beta-\beta_a)$	١	$\gamma/(\gamma-\gamma_a)$
6x6	64	0.004046	-0.0040	0.045769	-0.0544	0.005555	0.1148
8x8	100	0.004065	0.0007	0.050844	0.0504	0.003148	0.0650
10x10	144	0.004060	-0.0005	0.047080	-0.0273	0.002012	0.0416
12x12	196	0.004063	0.0002	0.049206	0.0166	0.001402	0.0290
14x14	256	0.004062	-0.0001	0.047468	-0.0193	0.001028	0.0212
16x16	324	0.004063	0.0001	0.048626	0.0046	0.000788	0.0163
18x18	400	0.004062	0.0000	0.047633	-0.0159	0.000622	0.0129
20x20	484	0.004062	0.0001	0.048363	-0.0008	0.000505	0.0104
22x22	576	0.004062	0.0001	0.047717	-0.0142	0.000417	0.0086
24x24	676	0.004062	0.0001	0.048218	-0.0038	0.000350	0.0072
26x26	784	0.004062	0.0001	0.047764	-0.0132	0.000298	0.0062

Dimensionless values: o the deflection at the central plate; ß the moment at the central point and ١ the moment at the mid support along x (or y), and their relative errors respect to the analytical values α_a, β_a and γ_a, respectively.

Analytical values: $\alpha_a = \frac{w_c}{\left[\frac{p\cdot(a\cdot b)^2}{D}\right]} = 0.004062$,, $\beta_a = \frac{M_c}{\left[\frac{p\cdot(a\cdot b)}{D}\right]} = 0.048403$, $\gamma_a = \frac{M_s}{\left[\frac{p\cdot(a\cdot b)}{D}\right]} = 0$,

where: $p = 0.001\ daN/mm^2$ is the uniformly distributed load; w_c is the displacement at the central point; M_c is the moment at the central point along x (or y); M_s is the moment at the mid edge along x (or y).

Table 2 provides the results for a square plate simply supported under a concentrated central load. The dimensionless values and the relative errors found in the central deflection and the central moment are reported in Table 2. Also, the moment value at the middle edge is reported, which should be theoretically zero. The bending moment at the center is dimensionless, calculated by dividing the moment over a small surface area to avoid singularity. Relative errors for the central deflection and central moment are also included. For a 26 x 26 the thin plate elements achieve relative errors of approximately 0.10% for deflection and 1.64% for the central moment. These results confirm the method's accuracy even with fewer points.

Table 3 presents a summary of the results for a square plate that is fully clamped and subjected to a uniform loading condition. Dimensionless values of the central deflection, central moment, and the moment at the middle edge are reported, along with their respective relative errors. For a 26 x 26 mesh, the relative errors converge to 0.41% for the central deflection and 2.38% for the central moment, indicating good performance by the proposed method.

Table 2: Square plate supported on four edges, subjected to central point load.

Mesh	d.o.f.	o	$\alpha/(\alpha-\alpha_a)$	ſ	$\beta/(\beta-\beta_a)$	١	$\gamma/(\gamma-\gamma_a)$
6x6	64	0.011316	-0.0245	0.028773	-0.3992	-0.002794	-0.0583
8x8	100	0.011459	-0.0122	0.032893	-0.3132	-0.001739	-0.0363
10x10	144	0.011510	-0.0078	0.035631	-0.2560	-0.001259	-0.0263
12x12	196	0.011541	-0.0051	0.037986	-0.2068	-0.000856	-0.0179
14x14	256	0.011556	-0.0038	0.039785	-0.1693	-0.000670	-0.0140
16x16	324	0.011567	-0.0028	0.041436	-0.1348	-0.000483	-0.0101
18x18	400	0.011574	-0.0022	0.042787	-0.1066	-0.000400	-0.0084
20x20	484	0.011580	-0.0018	0.044066	-0.0799	-0.000302	-0.0063
22x22	576	0.011583	-0.0014	0.045155	-0.0571	-0.000262	-0.0055
24x24	676	0.011586	-0.0012	0.046196	-0.0354	-0.000204	-0.0043
26x26	784	0.011588	-0.0010	0.047108	-0.0164	-0.000183	-0.0038

Dimensionless values: o of the deflection at the central plate; ſ the moment at the central point and ١ the moment at the mid support along x (or y), and their relative errors respect to the analytical values α_a, β_a and γ_a, respectively.

Analytical values: $\alpha_a = \frac{w_c}{\left[\frac{P\cdot(a\cdot b)}{D}\right]} = 0.01160$, $\beta_a = \frac{M_c}{\left[\frac{P\cdot(a\cdot b)}{D}\right]} = 0.047892$, $\gamma_a = \frac{M_s}{\left[\frac{P\cdot(a\cdot b)}{D}\right]} = 0$,

where: $P = 100$ daN is the central point load; w_c is the displacement at the central point; M_c is the moment at the central point along x (or y), by referring F to a small area; M_s is the moment at the mid edge along x (or y).

Table 3: Square plate clamped on four edges, subjected to uniform load.

Mesh	d.o.f.	o	$\alpha/(\alpha-\alpha_a)$	ſ	$\beta/(\beta-\beta_a)$	١	$\gamma/(\gamma-\gamma_a)$
6x6	64	0.001214	-0.0362	0.017269	-0.2537	-0.040694	-0.2069
8x8	100	0.001264	0.0030	0.027893	0.2054	-0.046191	-0.0998
10x10	144	0.001258	-0.0015	0.020783	-0.1019	-0.047517	-0.0739
12x12	196	0.001265	0.0039	0.025128	0.0859	0.048908	-1.9532
14x14	256	0.001263	0.0027	0.021814	-0.0573	-0.049405	-0.0371
16x16	324	0.001265	0.0041	0.024158	0.0440	-0.049940	-0.0267
18x18	400	0.001265	0.0036	0.022242	-0.0388	-0.050171	-0.0222
20x20	484	0.001265	0.0042	0.023706	0.0244	-0.050431	-0.0171
22x22	576	0.001265	0.0040	0.022459	-0.0294	0.050557	-1.9853
24x24	676	0.001265	0.0042	0.023461	0.0139	-0.050701	-0.0119
26x26	784	0.001265	0.0041	0.022588	-0.0238	-0.050782	-0.0103

Dimensionless values: o the deflection at the central plate; ſ the moment at the central point and ١ the moment at the mid support along x (or y), and their relative errors respect to the analytical values α_a, β_a and γ_a, respectively.

Analytical values: $\alpha_a = \frac{w_c}{\left[\frac{p\cdot(a\cdot b)^2}{D}\right]} = 0.00126$, $\beta_a = \frac{M_c}{\left[\frac{p\cdot(a\cdot b)}{D}\right]} = 0.02314$, $\gamma_a = \frac{M_s}{\left[\frac{p\cdot(a\cdot b)}{D}\right]} = -0.05130$,

where: $p = 0.001$ daN/mm^2 is the uniformly distributed load; w_c is the displacement at the central point; M_c is the moment at the central point along x (or y); M_s is the moment at the mid edge along x (or y).

The results for a square plate fully clamped and subjected to a concentrated load at the center are shown in Table 4. Due to the singularity of the dimensionless central bending moment under a point load, this value is not computed. The central deflection and the moment at the middle edge are reported along with their relative errors. Remarkably, for a 26 x 26 mesh, the relative error for central deflection reduces to 0.02%, while the moment at the middle edge achieves an error of 0.00%. These results emphasize the high accuracy of the proposed formulation. Notably, the present method gives results that are close to the corresponding analytical values.

The presented results validate the effectiveness of the proposed finite element method. Despite using a reduced number of points, the thin plate elements demonstrate accuracy across all analyzed cases. The relative errors for deflection and moments consistently decrease with mesh refinement, showcasing the method's convergence and reliability. The proposed approach yields results for deflection that closely match the corresponding analytical values, confirming its suitability for thin plate analysis under various loading and boundary conditions.

Table 4: Square plate clamped on four edges, subjected to central point load.

Mesh	d.o.f.	o	$\alpha/(\alpha-\alpha_a)$	ſ	$\beta/(\beta-\beta_a)$	١	$\gamma/(\gamma-\gamma_a)$
6x6	64	0.005217	-0.0685	-	-	-0,094206	-0,2505
8x8	100	0.005474	-0.0224	-	-	-0,134384	0,0691
10x10	144	0.005505	-0.0170	-	-	-0,112838	-0,1023
12x12	196	0.005552	-0.0085	-	-	-0,131178	0,0436
14x14	256	0.005563	-0.0066	-	-	-0,119755	-0,0473
16x16	324	0.005579	-0.0038	-	-	-0.129894	0.0334
18x18	400	0.005584	-0.0029	-	-	-0.122996	-0.0215
20x20	484	0.005591	-0.0016	-	-	-0.129271	0.0284
22x22	576	0.005594	-0.0011	-	-	-0.124726	-0.0077
24x24	676	0.005597	-0.0005	-	-	-0.128941	0.0258
26x26	784	0.005599	-0.0002	-	-	-0.125696	0.0000

Dimensionless values: o the deflection at the central plate; ſ the moment at the central point and ١ the moment at the mid support along x (or y), and their relative errors respect to the analytical values α_a, β_a and γ_a, respectively.

Analytical values: $\alpha_a = \frac{w_c}{\left[\frac{P\cdot(a\cdot b)}{D}\right]} = 0.00560$, $\gamma_a = \frac{M_s}{\left[\frac{p\cdot(a\cdot b)}{D}\right]} = -0.1257$,

where: $P = 100$ daN is the central point load; w_c is the displacement at the central point; M_s is the moment at the mid edge along ɜ (or ɣ).

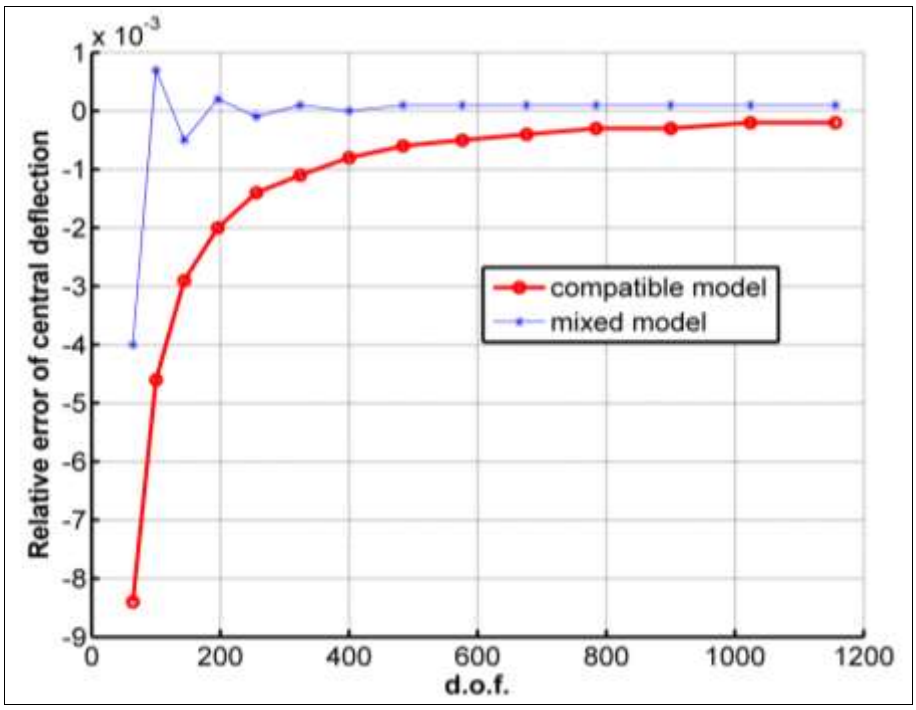

Fig 3: The relative error versus degree of freedom (d.o.f.) of central deflection for simply supported square plate uniformly loaded. Comparison between compatible (from an unpublished work of the authors) and mixed models.

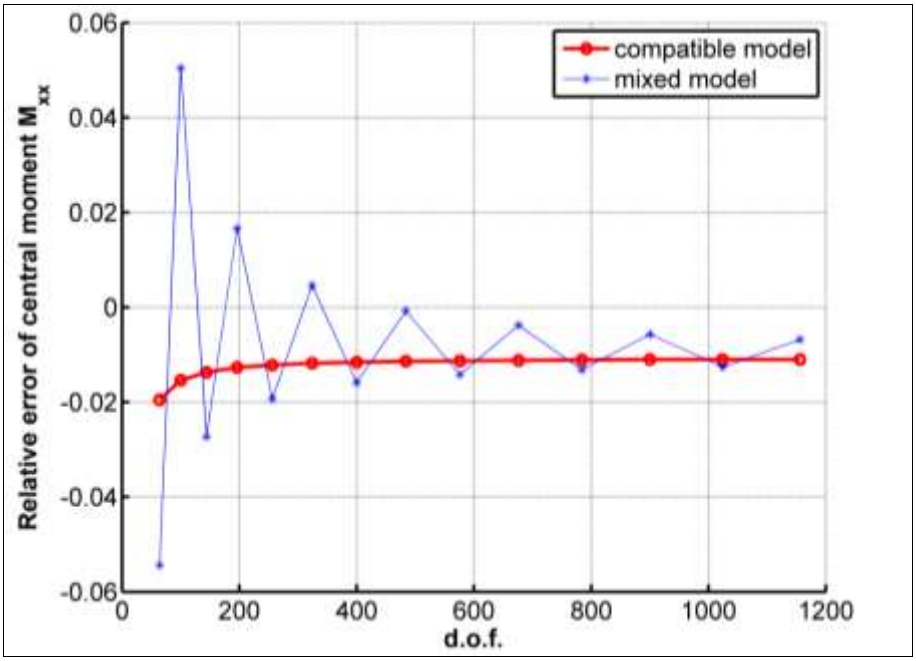

Fig 4: The relative error versus degree of freedom (d.o.f.) of central moment M_{xx} for simply supported square plate uniformly loaded. Comparison between compatible (from an unpublished work of the authors) and mixed models.

Conclusions

The proposed mixed finite element model demonstrates significant advantages over existing models, offering notable improvements in accuracy and versatility. A novel inter-continuity element for the analysis of 2D elastic problems has been developed, exhibiting high precision even with relatively coarse meshes. Validated for linear elastic materials, the model proves robust in addressing problems dominated by in-plane bending.

The mixed formulation, which combines bi-quadratic interpolation for displacements with bi-linear interpolation for moments, enhances the accuracy of stress field representation compared to standard compatible approaches. Numerical results obtained using the developed model confirm its capability to deliver precise solutions for both displacement and stress states of thin plates. As the mesh is refined, the displacement values converge closely to the exact solutions, exhibiting minimal errors. Similarly, the bending moments display excellent agreement with reference values, underscoring the model's strong performance in capturing variations across displacement and moment fields.

Moreover, the proposed framework offers significant potential for extension to a broader spectrum of problems, including shell elements, 3D continua, elastoplasticity, and dynamic analysis.

Acknowledgments

Vincenzo De Luca has developed the theoretical formulation, the Finite Element Method model and is author of the software code. Cosimo Marano has contributed to the elaboration of the numerical results.

References

1. Bathe KJ, editor. Finite Element Procedures. Prentice Hall; c1996.
2. Pian TH. Derivation of element stiffness matrices by assumed stress distributions. AIAA Journal. 1964;2(7):1333-1336.
3. Pian TH, Sumihara K. Rational approach for assumed stress finite elements. International Journal for Numerical Methods in Engineering. 1984;20(9):1685-1695.
4. Simo JC, Rifai M. A class of mixed assumed strain methods and the method of incompatible modes. International Journal for Numerical Methods in Engineering. 1990;29(8):1595-1638.
5. Bergan PG, Felippa CA. The first ANDES elements: 9-dof plate bending triangles. Computer Methods in Applied Mechanics and Engineering. 1991;93(2):217-246.
6. Boussem F, Belounar L. A Plate Bending Kirchhoff Element Based on Assumed Strain Functions. Journal of Solid Mechanics. 2020, 12(4).
7. Rebiai C, Belounar L. An effective quadrilateral membrane finite element based on the strain approach. Measurement. 2014;50:263-269.
8. Liu GR, Nguyen-Thoi T, Nguyen-Xuan HB, Lam KY. A node-based smoothed finite element method (NS-FEM) for upper bound solutions to solid mechanics problems. Computers and Structures. 2009a;87(1-2):14-26.
9. Liu GR, Nguyen-Thoi T, Lam KY. An edge-based smoothed finite element method (ES-FEM) for static, free, and forced vibration analyses of solids. Journal of Sound and Vibration. 2009b;320(4–5):1100-1130.
10. Zienkiewicz O, Taylor R. The Finite Element Method. Volume 1: The basis. Butterworth-Heinemann, Oxford; c2000a.
11. Zienkiewicz O, Taylor R. The Finite Element Method. Volume 2: Solid mechanics. Butterworth-Heinemann, Oxford; c2000b.
12. Pian TH, Tong P. Basis of finite element methods for solid continua. International Journal for Numerical Methods in Engineering. 1969;1(1):3-28.
13. Lee SW, Pian TH. Improvement of plate and shell finite elements by mixed formulations. AIAA Journal. 1978;16(1):29-34.

14. Lee SW, Wong SC. Mixed formulation finite elements for Mindlin theory plate bending. International Journal for Numerical Methods in Engineering. 1982;18(9):1297-1311.
15. Leonetti L, Aristodemo M. A composite mixed finite element model for plane structural problems. Finite Elements in Analysis and Design. 2015;94:33-46.
16. Bilotta A, Casciaro R. A high-performance element for the analysis of 2D elastoplastic continua. Computer Methods in Applied Mechanics and Engineering. 2007;196(4–6):818-828.
17. Szilard R. Theory and analysis of plates: Classical and numerical methods. Englewood Cliffs, NJ: Prentice-Hall, Inc.; c1974. p. 728.
18. Timoshenko SP, Woinowsky-Krieger S. Theory of plates and shells. McGraw-Hill, New York; c1984.